

Drone Positioning From Combined mmWave Radar and Depth Camera Data

José A. Paredes¹, Miles Hansard², Khalid Z. Rajab^{2,3}, Fernando J. Álvarez¹ and Teodoro Aguilera¹

¹Sensory System Research Group (GISS), University of Extremadura, Av. de Elvas s/n, 06006 Badajoz, Spain.

²Centre for Advanced Robotics (ARQ), School of EECS, Queen Mary University of London, Mile End Road, London E1 4NS, UK.

³NodeNs Medical Ltd., 10 Bloomsbury Way, London WC1A 2SL, UK.

Abstract

Accurate positioning is needed for many drone manoeuvres, such as landing or remote manipulation. This work uses a millimeter-wave radar device to produce range-angle and range-velocity heatmaps. Additional depth data is obtained, while the drone is flying, from a time of flight camera. The radar and depth data are subsequently combined, using Gaussian process regression. This approach increases the accuracy of the proposed localization system, while preserving the advantages of the radar sensor in poor visibility conditions. An experimental evaluation of the system is performed, in a typical flight scenario.

Keywords

mmWave Radar, ToF Camera, local positioning system, UAV

1. Introduction

The development of reliable positioning systems for UAVs (unmanned aerial vehicles) has become essential, owing to the widespread use of these platforms. Recent examples include surveillance [1], logistical [2], audiovisual [3] and military [4] tasks. These applications require a positioning system of some kind, which provides input to the process for both detection and navigation purposes. These systems need to provide accurate coordinates, especially for certain manoeuvres, like landing or grasping.

This work describes a precise 3D drone positioning system, based on a mmWave (millimeter-wave) radar and a ToF (time of flight) camera. The main idea is to detect and localise the drone with the ToF camera, and then to use this data to calibrate the radar. The resulting system

IPIN'21: Eleventh International Conference on Indoor Positioning and Indoor Navigation, November 29 – December 11, 2021, Lloret de Mar, Spain

✉ japaredesm@unex.es (J. A. Paredes); miles.hansard@qmul.ac.uk (M. Hansard); khalid@nodens.eu (K. Z. Rajab); fafranco@unex.es (F. J. Álvarez); teoaguibe@unex.es (T. Aguilera)

🌐 <https://giss.unex.es/testimonial/jose-antonio-paredes-moreno-en/> (J. A. Paredes);

<http://www.eecs.qmul.ac.uk/~miles/> (M. Hansard); <https://nodens.eu/> (K. Z. Rajab);


<https://giss.unex.es/testimonial/fernando-javier-alvarez-franco-en/> (F. J. Álvarez);

<https://giss.unex.es/testimonial/teodoro-aguilera-benitez-en/> (T. Aguilera)

🆔 0000-0002-0412-0179 (J. A. Paredes); 0000-0002-7610-1452 (F. J. Álvarez); 0000-0001-9436-5999 (T. Aguilera)



© 2021 Copyright for this paper by its authors. Use permitted under Creative Commons License Attribution 4.0 International (CC BY 4.0).

 CEUR Workshop Proceedings (CEUR-WS.org)

benefits from the advantages of the mmWave and ToF devices, and covers the whole workspace of the drone.

The paper is organised as follows: the main related works are presented in Section 2; the proposed algorithm is developed in Section 3; the experimental setup is described in Section 4, along with the main results; finally, the conclusions and future works are indicated in Section 5.

2. Related Works

Radar systems have been widely used in the last decades to detect targets. Depending on the wavelength and beam spread, a radar can return multiple readings from the same transmission, leading to a spatial representation of the environment. By capturing the reflected signal, a radar system can determine the range, velocity, and AoA (angle of arrival).

Radar systems based on mmWave technology have become increasingly popular for spatial sensing tasks. These include detecting and tracking humans, in order to locate and protect them in potentially dangerous environments. For instance, the Doppler spectrum is analysed in [5] to distinguish the movement of people's limbs when walking and thus locate them. In particular, this system is able to differentiate the movement of an adult from that of a child. Also a fusion algorithm between mmWave and cameras RGB (red/green/blue) is shown in [6], where the image ROIs (regions of interest) are dynamically adapted according to the distance. Some research tries to achieve a position using only a mmWave device, such as [7]. Here, the authors apply a human gait recognition technique (the device used operates in the 77–81GHz band). After an initial setup stage, a spatial resolution of 4.4cm and a maximum unambiguous distance of 5m are achieved. In terms of velocity, the maximum radial velocity is 2m/s, with a resolution of 0.26m/s. In total, the algorithm works with a recognition accuracy of 89% with 12 people to identify and 0.16m positioning error.

A positioning and tracking system based on 60GHz signals is analysed in [8]. This design manages to filter out multiple reflections and diffuse scattering components so that the accuracy achieved is relatively high. Its working area extends from 0.46m to 5.55m in the longitudinal direction and from 1.91m on the left to 3.04m on the right. The target's position is obtained by calculating the local centroid of the associated point cloud. Globally, the system ensures a positioning in the plane, with a 99% confidence level and an error around 30–40cm.

There are also works whose target is a drone. For example, two approaches to perimeter surveillance are presented in [9]. This system covers distances from tens to hundreds of metres, and the authors show that velocity can be estimated, by analysing small Doppler shifts. Also, 2D detection and tracking for UAVs is explored in [10], where a comparison with a lidar system is made. The authors can detect drones at distances up to 25m, although if the environment contains clutter, the detection is lost at 5m. Besides, when the UAV must be detected at low flight angles, the multipath effect (due to reflection in ground clutter) could mask direct reflections from the target. Other works, such as [11, 12], focus on pursuit of one drone by another. In this scenario, a 2D radar mounted on the tracking drone is used to detect the target. The missing axis information is obtained via geometric calculations, by estimating the position of the first drone.

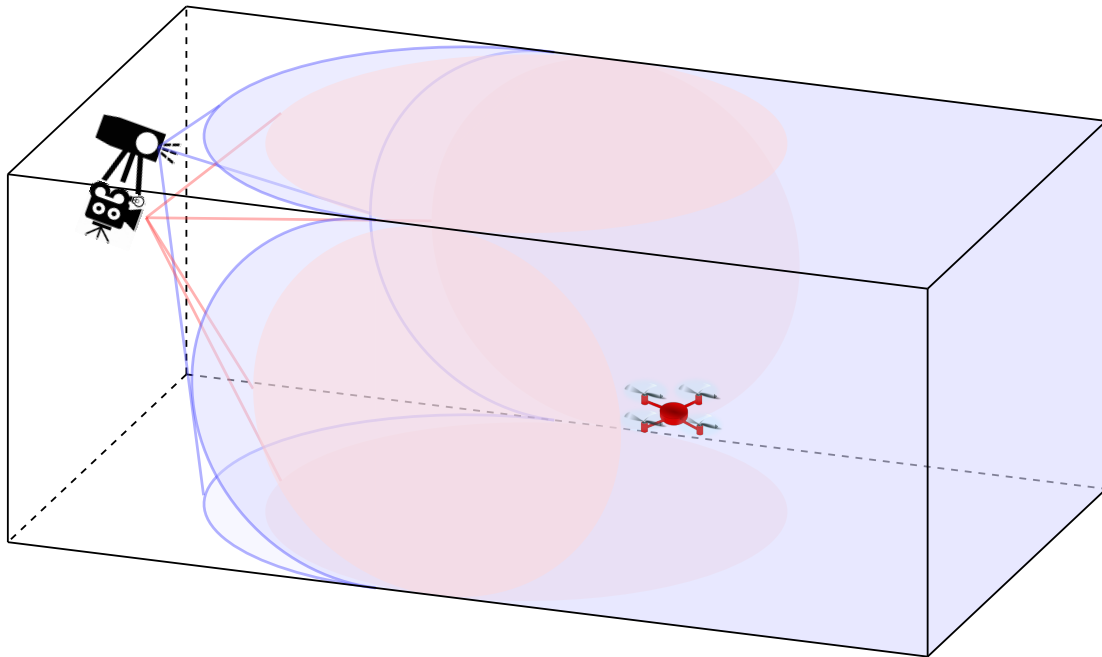


Figure 1: System overview. The ToF camera provides the drone coordinates, from a limited FoV, that will be used to calibrate the mmWave radar. The latter has full coverage of the scene.

3. Proposed LPS

The main objective of this work lies in implementing an LPS (local positioning system) to localise a drone flying in a cluttered scene. We use a mmWave radar, which has the following advantages. Firstly, it works in the absence of visible light, and performs well under challenging environmental conditions (e.g. fog, smoke, rain). Secondly, these devices effectively preserve privacy, as they do not provide recognisable images, but only a map of reflected energy.

This LPS is designed to work in relatively small spaces, focused on addressing those manoeuvres needing high accuracy, such as landing or taking off. Based on that, the mmWave radar will be calibrated using the data from a ToF camera. The main idea is to use the high accuracy of the camera, which has a limited maximum range and FoV (field of view), to calibrate the data from the radar. The main steps for the algorithm are detailed in the following sections.

3.1. Depth camera target detection

The idea to get 3D accurate coordinates for calibration is to adapt the algorithm in [13] to detect the flying drone in a scene where the ToF camera is arranged with the radar, as indicated in Figure 1. This camera will provide the data for the red shaded area, which will be used as input to a supervised learning algorithm – Section 3.3 – for the radar to work over the whole scene (blue shaded area).

In [13], the authors consider the disturbance that a quadcopter causes in a azimuthal depth map so as to apply a 2D matched filter, known as “Gnome Hat”. This wavelet allows the system

to detect all drones flying in the scene quickly. Moreover, it is dynamically adapted to the image portion that they occupy, taking into account the variation of this parameter with their flying altitude, which is also theoretically determined. The filter has been conveniently adapted to detect drones in a tilted position, taking into account the size of the drone used and the image produced (see Section 4 for more details on this device).

3.2. Radar target detection

Once the radar data have been acquired, the detection must be strengthened, in order to discount the effects of clutter in the scene, which can obscure the drone. This process is done in three stages:

1. By fitting a simple aluminium retro-reflector to the drone, thereby increasing the target RCS (radar cross-section).
2. By subtracting the static background signal, once the data has been acquired. This technique can be applied to velocity as well as position maps.
3. By using the micro-Doppler effect. When an object has some mechanical vibration or rotation, a modulation in frequency is induced in the reflected wave, generating side-lobes around the base frequency, allowing us to distinguish the range at which the drone is flying.

3.3. Localization algorithm

The fundamental concept in radar systems is the emission of a signal and its reception after reflecting from the surrounding objects. Specifically, the device chosen in this work is based on a MIMO (multiple input multiple output) approach, which uses digital beamforming to optimise the angular estimates.

Briefly, two consecutive operations of spectral analysis are required to obtain information from radar data. One determines the range and the velocity, and the other one extracts angular information (azimuth and elevation if the antenna layout allows it). Here, the first analysis will be through a FFT (fast Fourier transform), while MUSIC (multiple signal classification) will be applied for the extraction of angles. For more in-depth radar basics, see [14].

The data read from the device can be summarise as follows. Let $\mathbf{P} \equiv P(r, \theta, \phi)$ be the 3D range-azimuth-elevation array obtained after both spectral analysis over space, as explained in Section 3.2, and $\mathbf{P}_D \equiv P_D(r, v)$ the 2D range-velocity array after one spectral analysis over time (MIMO strategy [15, 16]). Both arrays have previously gone through the background subtraction stage. Thus, the following representations can then be constructed:

- A range-azimuth heatmap:

$$P_A(r, \theta) = \max_{\phi} P(r, \theta, \phi) \quad (1)$$

- A range-elevation heatmap:

$$P_E(r, \phi) = \max_{\theta} P(r, \theta, \phi) \quad (2)$$

- A range profile:

$$P_D(r) = \text{mean}_v P_D(r, v) \quad (3)$$

Note that the last equation calculates the average over the velocity. In this way, the sidelobes mentioned above (Section 3.2) help increase the main peak of this profile, i.e., the detection is strengthened. Then, the range coordinate can be taken as:

$$r_+ = \arg \max_r P_D(r) \quad (4)$$

In the same way, considering the coordinate r_+ , the angular coordinates can be extracted:

$$\theta_+ = \arg \max_{\theta} P_A(r_+, \theta) \quad (5)$$

$$\phi_+ = \arg \max_{\phi} P_E(r_+, \phi) \quad (6)$$

Alternatively, we can use a more sophisticated method, to estimate the 3D position from the radar data arrays. In particular, we use a GPR (Gaussian process regression) over the angular profiles $P_A(r_+, \theta)$ and $P_E(r_+, \phi)$ to try to improve the global accuracy. The hypothesis is that the GPR estimates $[\theta_*, \phi_*]$ will be better than the direct maximum estimates $[\theta_+, \phi_+]$ in (5) and (6):

$$\theta_* \leftarrow \text{GPR}_{\theta}(r_+, \alpha, \epsilon) \quad (7)$$

$$\phi_* \leftarrow \text{GPR}_{\phi}(r_+, \alpha, \epsilon) \quad (8)$$

where α and ϵ are the coefficients representing the former profiles in a B-spline basis. This is done to reduce the input size in the GPR. Besides, this procedure will absorb the lack of calibration between the ToF camera and the radar. The same procedure will be assessed for range:

$$r_* \leftarrow \text{GPR}_r(r_+, \alpha, \epsilon) \quad (9)$$

4. Experimental setup and results

This section presents the experimental setup as well as the main results to assess the proposed LPS. There are a range of devices that could address the problem described here. We have implemented the system as affordably as possible, using two off-the-shelf devices: a PMD Picoflexx [17] ToF camera, and a Texas Instruments IWR6843ISK-ODS mmWave radar [18]. These devices are mounted as shown in Figure 2, and slightly tilted, with respect to the ground, for better radar performance.

The target is a Parrot Mambo Minidrone [19], a small UAV with a wingspan of 13cm. The small size of this drone is deliberately challenging for any localisation system. As commented in Section 3.2, an aluminium retroreflector is attached to the drone, in order to increase the RCS, as shown in Figure 3. This piece has been wrapped in white paper to avoid the ToF camera becoming saturated due to the high reflectivity of the aluminium. Note that the radar signal will not be affected by this covering.

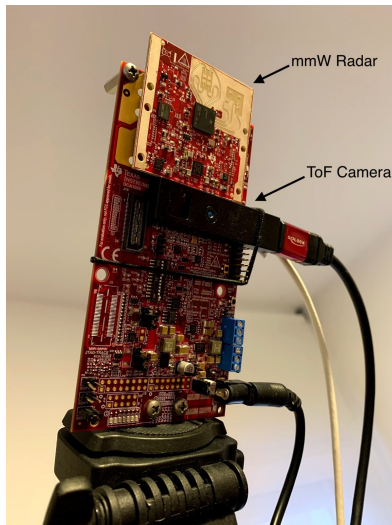


Figure 2: Experimental setup. The ToF camera has been attached to the mmWave radar, in order to calibrate the system.

Firstly, the background subtraction stage is tested. Figure 4 depicts raw heatmaps (top), compared to the results after background subtraction (bottom). It can be seen that this is an effective way to remove clutter.

The detection can fail even after background subtraction, for example, due to the uncontrolled multipath effect suffered in these environments. The micro-Doppler effect is used to avoid this, as illustrated in Figure 5. If we relied only on the range-azimuth heatmap in Figure 5a, the detection would be erroneous. However, when the sidelobes generated from the propellers in the range-velocity heatmap (Figure 5b) are integrated, the detection is corrected, as can be extracted from the red line in Figure 5c.

Finally, a simultaneous record from the camera and the radar is taken while the drone is flying. The positioning results are depicted in figure 6 for range, azimuth and elevation separately.



Figure 3: Parrot Mambo Minidrone, with a trihedral retroreflector to increase mmWave detectability.

Here, the points represent the values obtained by extracting the maxima of all radar profiles $[r_+, \theta_+, \phi_+]$ versus the values obtained with the camera. It can be seen that the range maxima are close to the directly estimated values (45° line). The angular estimates are more scattered, and a systematic pattern of errors can be seen. In order to address this, a GPR has been performed on these measurements, as represented by the blue line and the shaded area. This line allows us to notice the slight bias due to the mis-calibration between both devices, which will be absorbed by the final GPR.

Now, the data is randomly divided into 70% training and 30% test data, represented respectively as red and blue points in the last figure. New GPRs whose inputs are those proposed in equations (7), (8) are implemented. For range, it has been experimentally found that the results are slightly better when employing the next regression, instead of equation 9:

$$r_* \leftarrow \text{GPR}_r(r_+) \quad (10)$$

The final results are shown in Figure 7. The x -axis represents the coordinates extracted from the camera $[R, \Theta, \Phi]$, while the y -axis corresponds to the estimates from the GPR. It can be observed that the scattering has been reduced, i.e., the RMSE (root-mean-square error) has

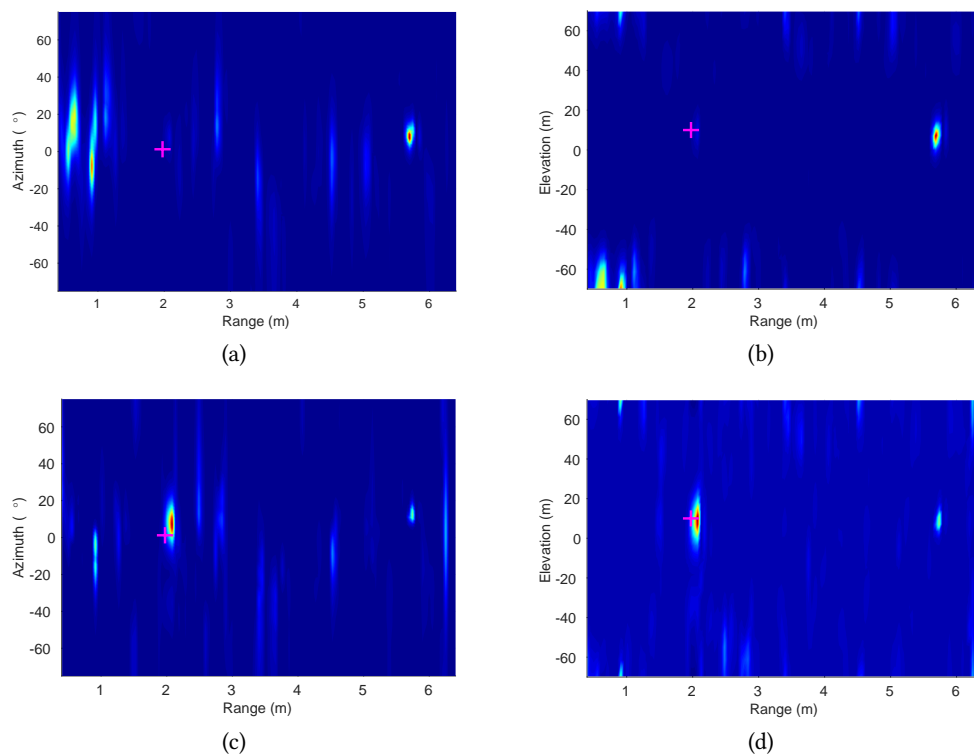


Figure 4: Background subtraction example for azimuth (a,c), and elevation (b,d) heatmaps. The magenta cross indicates the true position of the target. Environmental clutter produces false peaks in (a,b), which dominate the target. After background subtraction in (c,d), the dominant peak is close to the true position (estimated by the camera system). The residual biases are modelled by GPR.

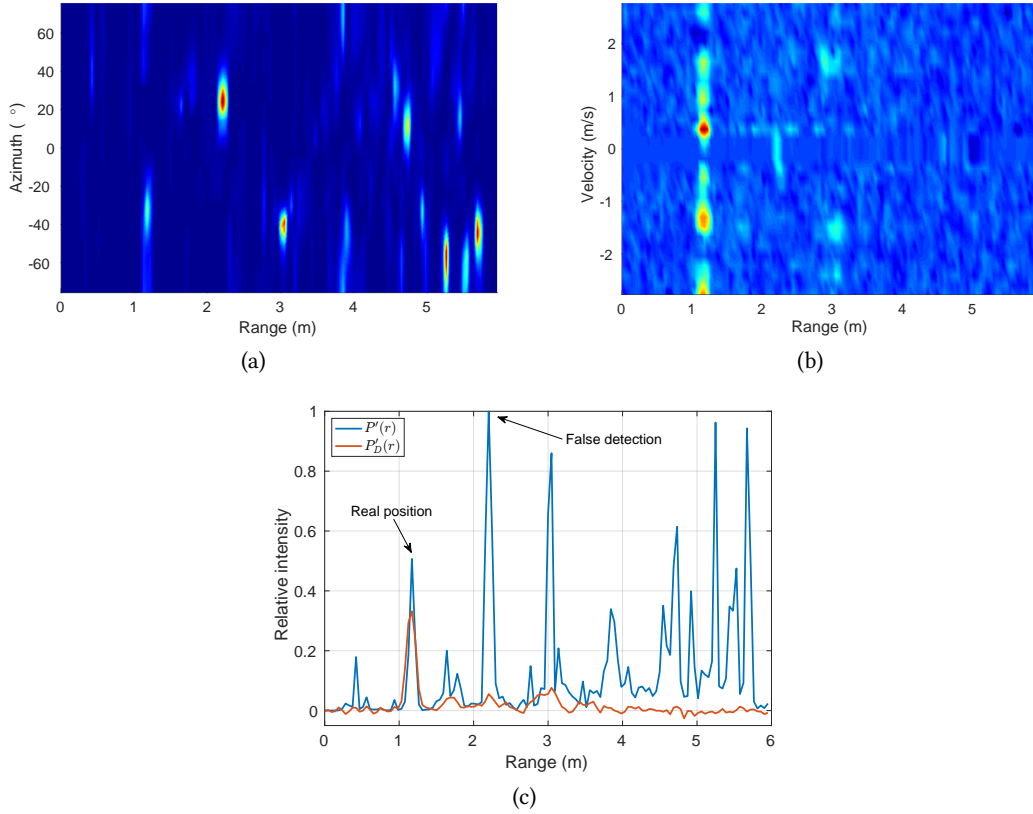


Figure 5: Example use of micro-Doppler information to assist target detection. The peak of the range profile extracted from the range-azimuth heatmap (a), around 3m, does not correspond to the true target range. However, the peak of the range-velocity data (b) is located at the true range of the target (c).

Table 1

Summary of RMSEs for the proposed LPS.

	Direct Maxima	Final GPR
Range (cm)	19.40	14.74
Azimuth (°)	7.75	7.48
Elevation (°)	8.62	4.11

improved, as shown in Table 1.

5. Conclusions and future work

This paper has presented an LPS based on a mmWave radar sensor, which has been dynamically calibrated with respect to a ToF camera. In this way, the advantages of each device are combined, while their drawbacks are compensated for.

The main proposal lies in implementing a GPR over the radar data, whose inputs are concate-

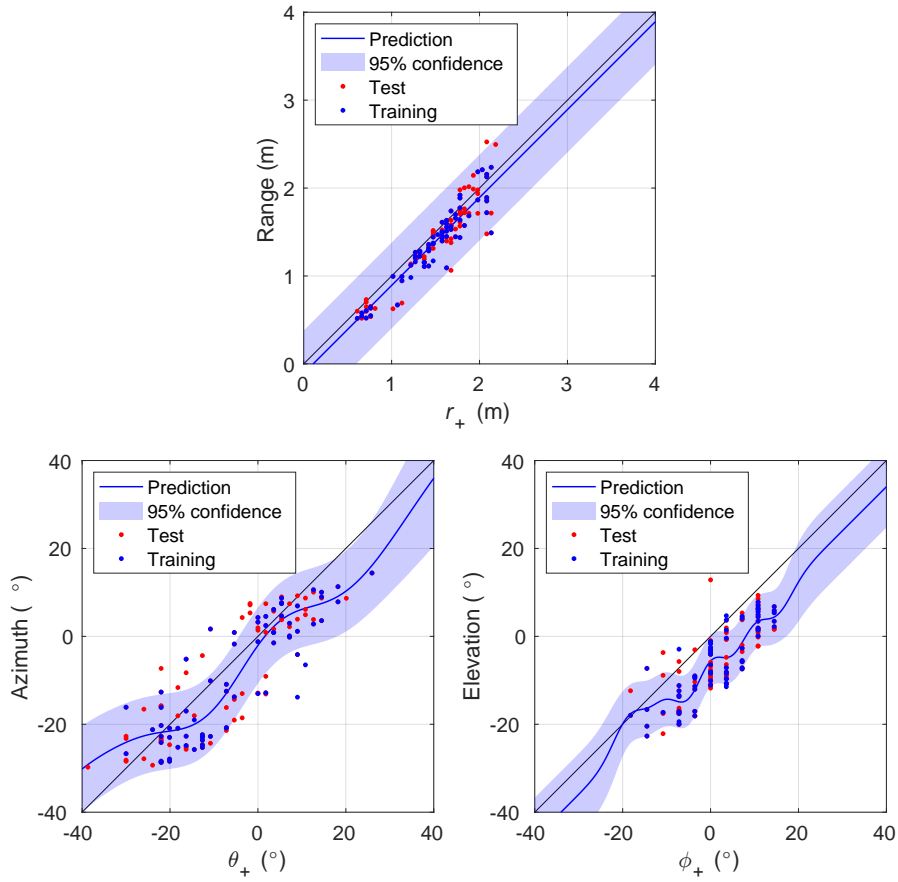


Figure 6: Positioning results r_+ , θ_+ and ϕ_+ directly taken from the maxima of the respective profiles. The regression line of all the points (blue line) reveal a slight bias, probably due to the mis-calibration between the devices. The point colours represent training (red) and test (blue) data for the final GPR shown in figure 7.

nated versions of range, azimuth and elevation data, taking into account that a combination of those defines every point in the space. The ground truth has been provided by a ToF camera in a precise way. The system has been experimentally tested, and it has been demonstrated that the experimental RMSE decreases for range and angular estimates. Future work will investigate different beamforming techniques for processing the radar data, as well as alternative supervised learning algorithms for the calibration process.

Acknowledgments

This work has been partially supported by the UK EPSRC National Centre for Nuclear Robotics (NCNR) EP/R02572X/1; by the Spanish Government and the European Regional Development Fund (ERDF) through Project MICROCEBUS under Grant RTI2018-095168-B-C54; and by the Regional Government of Extremadura and ERDF - ESF, under Project GR18038 and through the

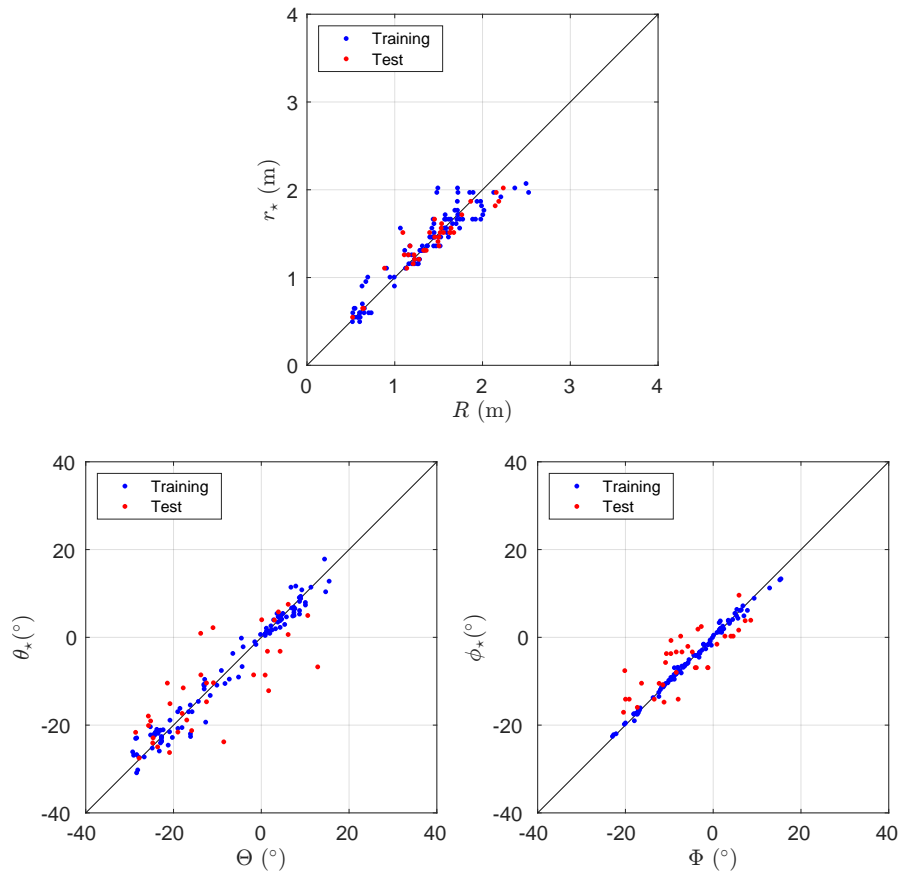


Figure 7: Results for the final GPR, where the inputs have been taken as $[r_+, \alpha, \epsilon]$. A narrowing in the dispersion of the data can be observed, which leads to a decrease in the RMSE.

Pre-Doctoral Scholarship under Grant 45/2016 Exp. PD16030.

References

- [1] S. K. Boddhu, M. McCartney, O. Ceccopieri, R. L. Williams, A collaborative smartphone sensing platform for detecting and tracking hostile drones, in: T. Pham, M. A. Kolodny, K. L. Priddy (Eds.), SPIE Defense, Security, and Sensing, Baltimore, Maryland, USA, 2013, p. 874211. doi:10.1117/12.2014530.
- [2] R. Kellermann, T. Biehle, L. Fischer, Drones for parcel and passenger transportation: A literature review, *Transportation Research Interdisciplinary Perspectives* 4 (2020) 100088. doi:10.1016/j.trip.2019.100088.
- [3] J. Harvard, M. Hyvönen, I. Wadbring, Journalism from Above: Drones and the Media in Critical Perspective, *Media and Communication* 8 (2020) 60–63. doi:10.17645/mac.v8i3.3442.
- [4] T. de Swarte, O. Boufous, P. Escalle, Artificial intelligence, ethics and human values: The

- cases of military drones and companion robots, *Artificial Life and Robotics* 24 (2019) 291–296. doi:10.1007/s10015-019-00525-1.
- [5] Y. Balal, N. Balal, Y. Richter, Y. Pinhasi, Time-frequency spectral signature of limb movements and height estimation using micro-doppler millimeter-wave radar, *Sensors* 20 (2020) 4660. doi:10.3390/s20174660.
- [6] X.-p. Guo, J.-s. Du, J. Gao, W. Wang, Pedestrian detection based on fusion of millimeter wave radar and vision, in: *2018 International Conference on Artificial Intelligence and Pattern Recognition, AIPR 2018*, ACM, New York, USA, 2018, pp. 38–42. doi:10.1145/3268866.3268868.
- [7] P. Zhao, C. X. Lu, J. Wang, C. Chen, W. Wang, N. Trigoni, A. Markham, mID: Tracking and identifying people with millimeter wave radar, in: *2019 15th International Conference on Distributed Computing in Sensor Systems (DCOSS)*, IEEE, Santorini Island, Greek, 2019, pp. 33–40. doi:10.1109/DCOSS.2019.00028.
- [8] A. Antonucci, M. Corra, A. Ferrari, D. Fontanelli, E. Fusari, D. Macii, L. Palopoli, Performance Analysis of a 60-GHz Radar for Indoor Positioning and Tracking, in: *2019 International Conference on Indoor Positioning and Indoor Navigation (IPIN)*, IEEE, Pisa, Italy, 2019, pp. 1–7. doi:10.1109/IPIN.2019.8911764.
- [9] M. Caris, S. Stanko, W. Johannes, S. Sieger, N. Pohl, Detection and tracking of Micro Aerial Vehicles with millimeter wave radar, in: *Proceedings of the 2016 European Radar Conference (EuRAD)*, London, UK, 2016, pp. 406–408.
- [10] M. U. de Haag, C. G. Bartone, M. S. Braasch, Flight-test evaluation of small form-factor LiDAR and radar sensors for sUAS detect-and-avoid applications, in: *2016 IEEE/AIAA 35th Digital Avionics Systems Conference (DASC)*, Sacramento, California, UK, 2016, pp. 1–11. doi:10.1109/DASC.2016.7778108.
- [11] S. Dogru, R. Baptista, L. Marques, Tracking drones with drones using millimeter wave radar, in: *Robot 2019: Fourth Iberian Robotics Conference*, volume 1093, Oporto, Portugal, 2019, pp. 392–402. doi:10.1007/978-3-030-36150-1_32.
- [12] S. Dogru, L. Marques, Pursuing drones with drones using millimeter wave radar, *IEEE Robotics and Automation Letters* 5 (2020) 4156–4163. doi:10.1109/LRA.2020.2990605.
- [13] J. A. Paredes, F. J. Álvarez, T. Aguilera, F. J. Aranda, Precise drone location and tracking by adaptive matched filtering from a top-view ToF camera, *Expert Systems with Applications* 141 (2020) 112989. doi:10.1016/j.eswa.2019.112989.
- [14] M. A. Richards, *Fundamentals of Radar Signal Processing*, McGraw Hill Professional, 2005.
- [15] E. Fishler, A. Haimovich, R. Blum, D. Chizhik, L. Cimini, R. Valenzuela, MIMO radar: An idea whose time has come, in: *Proceedings of the 2004 IEEE Radar Conference (IEEE Cat. No.04CH37509)*, 2004, pp. 71–78. doi:10.1109/NRC.2004.1316398.
- [16] J. Li, P. Stoica, MIMO Radar with Colocated Antennas, *IEEE Signal Processing Magazine* 24 (2007) 106–114. doi:10.1109/MSP.2007.904812.
- [17] PMD, Flexx | picofamily, 2021. URL: <https://pmdtec.com/picofamily/flexx/>.
- [18] T. Instruments, IWR6843ISK-ODS IWR6843 intelligent mmWave overhead detection sensor (ODS) antenna plug-in module, 2020. URL: <http://www.ti.com/tool/IWR6843ISK-ODS>.
- [19] Parrot, Parrot Bebop 2 Power - Pack FPV, 2017. URL: <https://www.parrot.com/es/drones/parrot-bebop-2-power-pack-fpv>.